J. Fluid Mech. (1975), *vol.* 70, *part* 2, *pp.* 229–250
Printed in Great Britain

On the wave structure of the wall region of a turbulent boundary layer

By FRITZ H. BARK

Department of Mechanics, Royal Institute of Technology, Stockholm

(Received 4 October 1974)

Following the ideas suggested by Landahl (1967, 1975), some model calculations of the fluctuating velocity field in the wall region of a turbulent boundary layer have been carried out. It was assumed that the turbulent stresses are generated intermittently on small scales in time and space owing to bursting-type motions. The Reynolds-stress distribution during bursting periods and the mean velocity profile were assumed to be known, and the linear large-scale response to a random system of bursts was computed using an idealized model for the joint probability distribution in time and space of the occurrence of bursts. Computed energy spectra of the streamwise velocity fluctuations display scales in the spanwise and streamwise directions and time which are in good agreement with measurements by Morrison, Bullock & Kronauer (1971). However, the wavenumber bandwidths of the computed spectra are narrower than those of the measured ones. This discrepancy is probably due to the crudeness of the model employed for the Reynolds stress during bursting.

1. Introduction

It has been shown by Landahl (1967) that the propagation characteristics, i.e. convection velocity and decay rate, of the statistically dominant parts of the fluctuating pressure and normal velocity in a turbulent boundary layer are given by the phase velocity and decay rate, respectively, of slightly damped Tollmien–Schlichting waves that propagate in the mean shear flow. These waves were assumed to be excited by intensive small-scale bursting motions of the type discovered by Kline *et al.* (1967). However, Landahl's theory was not able to give the characteristic scales of the dominant fluctuations, only that the relation between the length and time scales in Fourier space is given by the dispersion relation for the damped Tollmien–Schlichting waves. The theoretical results agreed well with surface pressure measurements by Willmarth & Wooldridge (1962). The experimental work by Morrison & Kronauer (1969) and Morrison *et al.* (1971) clearly indicates that the statistically dominant streamwise fluctuations also have a wavelike character, thus lending further support to Landahl's (1967) waveguide model. The present work is an attempt to compute the dominant eddy scales in the wall layer, taken to be given by the peaks in the respective long-time averaged spectra, using a highly idealized model for the production mechanism. In § 2 some experimental work supporting the model used is briefly

discussed. In § 3 a recapitulation of the conceptual model of shear-flow turbulence suggested by Landahl (1975) is given. The statement of the problem and the governing equations are given in § 4. The strong nonlinear effects which occur during bursting periods are discussed in § 5. In this section the statistics of the bursting motions are also discussed. The computation of the energy spectra is described in § 6. In § 7 the results are discussed and compared with experiments.

2. Observations of the structure of boundary-layer turbulence

That the fluctuating velocity field in the wall region of a turbulent boundary layer possesses a high degree of organization was discovered by Kline and his group at Stanford University (Kline *et al.* 1967). As this region of the boundary layer is the one where the turbulent production attains its maximum, this discovery seemed to indicate that shear-flow turbulence is to a large degree of a deterministic nature. Kline *et al.* (1967) also inferred from their experiments that the turbulent momentum transport and production takes place intermittently in time and space through small-scale bursting motions. This was further established by Kim, Kline & Reynolds (1971). The dominant structure of the fluctuating velocity field in the wall layer was found to consist of long streaks of weak streamwise vorticity. After a fairly well-defined time each streak broke up through an intense small-scale bursting motion, which caused strong mixing and rapid growth of scales of motion. This bursting motion seemed to be the result of a hydrodynamic instability of the Kelvin–Helmholtz type associated with a local hydrodynamically unstable shear layer which was formed by the lifting up of low-speed fluid from a region near the wall by two counter-rotating vortices. A recent investigation by Offen & Kline (1974) indicates that there is a connexion between a burst and the one that occurred previously immediately upstream. This suggests that the bursts create new streaks which in turn produce new bursts and so on. Quantities such as the lifetime of the streaks, the average distance between streaks and the burst rate per unit span were shown by Kline *et al.* (1967) to be statistically reproducible.

A similar mechanism for the intermittent turbulent production and momentum transport was inferred by Corino & Brodkey (1969). They used a movie camera that could record the fluid motions near the wall, following the mean flow at any preselected distance from the wall. The bursting process (an expression not used by these authors) was found to start with a local deceleration of the fluid near the wall followed by an acceleration of the fluid slightly above, that is, a rather strong shear layer was formed near the wall. After the formation of this shear layer a small parcel of fluid was ejected very rapidly from the low-speed region up into the high-speed region, whereupon a significant growth of scales of motion took place. The bursting process ended with a sweeping motion of high-speed fluid from upstream towards the wall, which restored the instantaneous velocity profile to its mean value. Corino & Brodkey showed that the largest part of the total Reynolds stress was produced during the short bursting periods. The findings of Corino & Brodkey were further investigated by Wallace, Eckelmann & Brodkey (1972), who found that 140% of the Reynolds stress was produced

during the 'active' bursting periods and -40% by the 'passive' turbulent flow during the rest of the time. It should be pointed out that Corino & Brodkey (1969) did not find any indication of the presence of an unstable vorticity wave of the Kelvin–Helmholtz variety found by Kim *et al.* (1971). This discrepancy between the two investigations is, to this author's knowledge, unresolved at present. Otherwise the phenomena described seem to be very much of the same nature.

Several later investigations, e.g. those by Brodkey, Wallace & Eckelmann (1974), Blackwelder & Kaplan (1972) and Willmarth & Lu (1972, 1973), have given more detailed information on the intermittent bursting motions. The structure of the large-scale field near the wall was also investigated in detail by, among others, Bakewell & Lumley (1967), Morrison & Kronauer (1969), Morrison *et al.* (1971) and Gupta, Laufer & Kaplan (1971).

3. Brief description of the turbulence model employed

Guided by the experimental results discussed in § 2, Landahl (1975) has outlined a conceptual model of shear-flow turbulence. The essential idea in this model is that the large-scale eddies are excited by small-scale ones through the bursting mechanism. It is also hypothesized that the large eddies intermittently create conditions suitable for the occurrence of new bursts, thereby making the fluctuating fields self-sustaining. At its present stage of development, the model provides no closure scheme for the Reynolds equations, but merely tries to elucidate separately the physics of certain parts of the cycle described above. The dynamical coupling between the different scales of motion can at present only be treated in a qualitative manner. The key assumption in the mathematical formulation is that the nonlinear terms in the Navier–Stokes equations are of crucial importance only during bursting, i.e. locally during only a small fraction of the total time. Also the mean velocity field is regarded as known. The large-scale eddies are then computed in the Fourier space corresponding to the streamwise and spanwise directions and time. As was pointed out in § 1, proceeding in this manner Landahl (1967) computed frequency-filtered correlation lengths and convection velocities for surface pressure fluctuations which were in good agreement with experimental results by Willmarth & Wooldridge (1962).

For the small-scale field, assumed to be responsible for the main part of the turbulent momentum transport and production, the situation is much more complicated, because here nonlinearities are certainly of importance. Drawing on the similarity of the bursting process to the process of breakdown in the final stage of transition from laminar to turbulent flow in a boundary layer (see Klebanoff, Tidstrom & Sargent 1962), Landahl (1975) proposed that the bursting is due to focusing and trapping of small-scale secondary instability waves on the large-scale eddies. This would occur whenever the group velocity of the secondary waves becomes locally equal to the convection velocity of the flow inhomogeneity produced by the large-scale motions. This condition was used successfully by Landahl (1972) to predict the position of first appearance and frequency of the small-scale oscillations observed at the breakdown of the laminar instability wave.

If a turbulent boundary layer is regarded as a flow in a state of continuous transition one could in principle, according to this model, compute where and when bursting motions would occur if the large-scale field were given. However, this very complicated calculation has not yet been undertaken and further simplification seems to be necessary on this point. This part of the model dealing with the occurrence of bursts is not explicitly made use of in the present work, but has been briefly recapitulated for reference.

The Landahl (1975) model is related to the models proposed by Sternberg (1965) and Schubert & Corcos (1967) in that the fluctuating field is computed from an Orr–Sommerfeld equation. In the latter models the excitation mechanism for the velocity fluctuations near the wall is assumed to be provided by the surface pressure fluctuations emanating from large eddies further away from the wall. However, the recent experimental investigations referred to in the previous section, as well as many others, clearly indicate that the turbulent bursts are responsible for the main part of the production. Also, the surface pressure fluctuations scale on outer variables whereas the velocity fluctuations near the wall scale on inner variables, a circumstance which also favours the turbulent bursts as the excitation mechanism.

4. Statement of the problem

The problem considered is the flow of a viscous constant-density fluid over a rigid, impermeable, smooth, flat plate of large dimensions. Far above the plate the velocity of the fluid is assumed to be steady, uniform and parallel to the plate, i.e. no exterior pressure gradient is applied. The Reynolds number is assumed to be sufficiently large for a fully developed (self-similar) turbulent boundary layer to persist on the plate away from its edges. The problem to be considered is how the boundary-layer flow responds to an excitation caused by bursting motions which are compact in space and time and occur in a random manner near the plate. The mean velocity field is assumed to be known. Attention is focused on length scales which are large compared with the dimensions of the bursting regions. Also the time scales considered are larger than those typical of completion of the bursting motions. For computational reasons, see below, only the wall-layer region, i.e. the viscous sublayer and the buffer layer, is considered.

A Cartesian co-ordinate system is used The origin is located on the plate and the uniform mean velocity far away from the plate is in the x_1 direction. The x_2 direction is assumed to be perpendicular to the plate. In the usual way, the pressure and velocity fields are split into a mean and a fluctuating part according to

$$\Pi(x_k, t) = P(x_k) + p(x_k, t), \tag{1}$$

$$U_r(x_k, t) = V_r(x_k) + v_r(x_k, t), \tag{2}$$

where $P = \langle \Pi \rangle$, $V_r = \langle U_r \rangle$ and angular brackets denote ensemble averaging. In this work it is assumed that P is zero and that V_r is given by

$$V_r = \delta_{1r} a u_\tau [1 - \exp(-u_\tau x_2 / a\nu)], \tag{3}$$

as proposed by Schubert & Corcos (1967) as an approximate model for the mean velocity distribution near the wall in a turbulent boundary layer with zero pressure gradient. In (3) ν is the kinematic viscosity, a an adjustable constant and u_τ is the shear velocity, defined in the usual manner by $u_\tau = (\tau_w/\rho U_\infty^2)^{\frac{1}{2}}$, where τ_w is the viscous shear stress at the wall, ρ the fluid density and U_∞ the velocity of the exterior potential flow. It was shown by Schubert & Corcos (1967) that if the value of a is chosen to be 16 the expression (3) fits well the measurements by Coles (1956) of the streamwise mean velocity up to

$$u_\tau x_2/\nu \simeq 50,$$

but becomes increasingly worse further away from the wall. As only the wall region is to be considered, (3) is used in this work as a rough model. The reason for this simplification will be explained below. The length and velocity scales in (3) are $a\nu/u_\tau$ and au_τ, respectively, with a^2 serving as a Reynolds number, called R below, for the flow under consideration. Schubert & Corcos also discussed the parallel-flow assumption and showed that this approximation is a very good one.

With the use of the above length and velocity scales the Navier–Stokes equations in non-dimensional form become

$$U_{r,t} + U_s U_{r,s} = -\Pi_{,r} + R^{-1} U_{r,ss} \tag{4}$$

and the continuity equation

$$U_{r,r} = 0. \tag{5}$$

Taking the ensemble average of (4) and subtracting this average from (4), one finds after use has been made of (5)

$$v_{r,t} + V_1 v_{r,1} + \delta_{1r} v_2 V_{1,2} = -p_{,r} + R^{-1} v_{r,ss} + (\langle v_r v_s \rangle - v_r v_s)_{,s}, \tag{6}$$

$$v_{r,r} = 0. \tag{7}$$

For convenience, the following notation is introduced:

$$q_r = (\langle v_r v_s \rangle - v_r v_s)_{,s},$$

$$\mathbf{x} = (x, y, z), \quad \mathbf{v} = (u, v, w), \quad D = d/dy.$$

The vector $\mathbf{q}$ is assumed to be known in this work and is discussed in some detail in § 5. The system of equations (6) and (7) is to be solved subject to the usual no-slip condition and decay as y becomes large, i.e.

$$\mathbf{v} = 0 \quad \text{for} \quad y = 0,$$

$$\lim \mathbf{v} = 0 \quad \text{as} \quad y \to +\infty.$$

It turns out that further simplifications can be made if one considers the Fourier transform of (6) and (7) in the homogeneous directions and time and defines

$$\hat{\mathbf{v}} = (2\pi)^{-\frac{3}{2}} \int_{-\infty}^{+\infty} \exp\left[-i(\mathbf{k}.\mathbf{x}' - \omega t)\right] \mathbf{v}\, d\mathbf{x}'\, dt,$$

where $\mathbf{x}' = (x, z)$ and $\mathbf{k} = (k_x, k_z)$. The transforms of p and $\mathbf{q}$ are defined analogously. Insertion of the transformed variables into (6) and (7) gives directly

$$ik_x(U-c)\,\hat{u} + (DU)\,\hat{v} = -ik_x\hat{p} + R^{-1}(D^2 - k^2)\,\hat{u} + \hat{q}_x,$$

$$ik_x(U-c)\,\hat{v} = -D\hat{p} + R^{-1}(D^2 - k^2)\,\hat{v} + \hat{q}_y,$$

$$ik_x(U-c)\,\hat{w} = -ik_z\hat{p} + R^{-1}(D^2 - k^2)\,\hat{w} + \hat{q}_z,$$

$$ik_x\hat{u} + D\hat{v} + ik_z\hat{w} = 0,$$

where $c = \omega/k_x$ is the 'phase speed' in the streamwise direction of each Fourier component. It is convenient to introduce velocity components parallel and perpendicular to the vector $\mathbf{k}$ in the following manner (cf. Squire 1933):

$$k_x\tilde{u} = k_x\hat{u} + k_z\hat{w}, \quad k_x\tilde{w} = k_z\hat{u} - k_x\hat{w}. \tag{8), (9}$$

After some manipulations, one finds the following equations for $\hat{v}$ and $\tilde{w}$:

$$(U-c)(D^2-k^2)\hat{v} - (D^2U)\hat{v} + \frac{i}{k_xR}(D^2-k^2)^2\hat{v} = \frac{ik^2}{k_x}\hat{q}_y - D\left(\hat{q}_x + \frac{k_z}{k_x}\hat{q}_z\right), \tag{10}$$

$$(U-c)\tilde{w} + \frac{i}{k_xR}(D^2-k^2)\tilde{w} = \frac{ik_z}{k_x}(DU)\hat{v} - i(k_z\hat{q}_x - k_x\hat{q}_z)/k_x^2. \tag{11}$$

As $\hat{q}$ is assumed to be known (10) is an inhomogeneous Orr–Sommerfeld equation for $\hat{v}$. When $\hat{v}$ has been found (11) can be integrated directly to find $\tilde{w}$. Equation (10) can be solved in terms of the normal modes of the homogeneous Orr–Sommerfeld equation; see, for example, Eckhaus (1965, p. 107). If one defines a quantity $\hat{Q}$ as

$$\hat{Q} = \frac{ik^2}{k_x}\hat{q}_y - D\left(\hat{q}_x + \frac{k_z}{k_x}\hat{q}_z\right)$$

the solution of (10) can be written as

$$\hat{v} = -k_x \sum_n \left(\int_0^\infty \hat{Q}\tilde{v}^{(n)}\,dy \,/\, (\omega - \omega^{(n)})\, I_n \right) \hat{v}_n, \tag{12}$$

where I_n is given by

$$I_n = \int_0^\infty \tilde{v}^{(n)}(D^2-k^2)\hat{v}^{(n)}\,dy. \tag{13}$$

In (12), $\omega^{(n)}$ and $\hat{v}^{(n)}$ are the nth eigenvalue and eigenfunction respectively of the homogeneous Orr–Sommerfeld problem for a given $\mathbf{k}$ (in this case real). $\tilde{v}^{(n)}$ is the corresponding adjoint eigenfunction. Once $\hat{v}$ and $\tilde{w}$ are known, $\hat{u}$ and $\hat{w}$ may easily be obtained from the inversion of (8) and (9).

The appearance of the Orr–Sommerfeld operator in (10) is the reason for the choice of the expression (3) for the mean velocity profile because, as was shown by Schubert & Corcos (1967), the solution of the homogeneous Orr–Sommerfeld problem can then be very easily obtained in terms of an algebraically very simple Frobenius series in e^{-y}. Schubert & Corcos (1967) used a boundary-layer version of the Orr–Sommerfeld equation. In the present work the full equation was solved; for details the reader is referred to Bark (1974).

Equation (12) shows that the only singularities of $\hat{v}$ in the complex frequency plane are located at the eigenvalues of the Orr–Sommerfeld equation. This means that v has a wave structure. However, from (11) it can be seen that $\tilde{w}$ has, in addition to these poles in the frequency plane, singularities emanating from the inversion of the operator on the left-hand side of (11). These singularities correspond essentially to viscous decay of fluid motions parallel to the wall. A peculiar feature of these motions is their lack of pressure fluctuations; see Landahl (1975). Their presence will make the u spectra have a composite structure, i.e. both wave-

FIGURE 1. The uv component of the Reynolds-stress tensor as function of time at $y^+ = 30$. From Willmarth & Lu (1972).

like and convected eddy-like motions will be present. However, the experiments by Morrison *et al.* (1971) indicate that the wavy motions dominate and consequently the terms within the last parentheses in (11) are neglected in this heuristic analysis.

5. Discussion of the nonlinear terms

The forcing term on the right-hand side of (10), which describes the spatial variation of the difference between the averaged Reynolds stress and its instantaneous value, can be expected to be locally very large during bursting periods. The experiments by Kline *et al.* (1967), Corino & Brodkey (1969) and Willmarth & Lu (1972) suggest that the averaged terms in **q** can be neglected. In the theory of aerodynamic noise (Lighthill 1952), which has some similarities with the present one, a tractable mathematical problem can be formulated because the weak linear flow (sound waves) and the strongly nonlinear flow (turbulence) have a weak mutual interaction, the former motion being thought of as driven by the latter. The present problem is conceptually more complicated, but it is assumed that the intermittent spatial and temporal structure of the bursting motions is sufficiently distinct to allow the use of a simplified mathematical model for the forcing mechanism, which is assumed to excite the large-scale fluctuations in a 'sprinkling' manner, cf. Kovasznay (1973). However, it should be kept in mind that the mean time between bursts, scaled on wall variables, is an increasing function of the outer Reynolds number according to Rao, Narasimha & Badri Narayanan (1971) and Laufer & Badri Narayanan (1971). This implies that the proposed model is likely to work only at high Reynolds numbers based on outer variables. Such a case is shown in figure 1, from Willmarth & Lu (1972), which shows that the temporal behaviour at a fixed point in space of the fluctuating transport of streamwise momentum perpendicular to the wall resembles a sequence of Dirac delta functions.

There is, as yet, no conclusive information available regarding the size of the bursting regions. The intermittent momentum transport appears to take place over bounded continuous ranges of scales and strengths. However, Corino & Brodkey (1969) estimated the dimensions of the region of small-scale motion during the ejection phase as $\Delta x^+ \simeq 20$–40, $\Delta y^+ \simeq 15$–20 and $\Delta z^+ \simeq 5$–50. Kim *et al.* (1971) reported $\Delta z^+ \simeq 10$–30 as typical for the spanwise width of a burst. Morrison *et al.* (1971) found $\lambda_x^+ \simeq 630$ and $\lambda_z^+ \simeq 135$ as the characteristic wavelengths of the long-time averaged energy spectra near the wall. Consequently, there is a separation of length scales, which can be expected to increase with the Reynolds number. The same can be expected to hold for the corresponding time scales. Thus, it seems reasonable, as a rough model, to equate the dependence of the forcing term $\hat{Q}$ on the homogeneous space co-ordinates and time to a sequence of randomly distributed Dirac delta functions.

The dependence of $\hat{Q}$ on the co-ordinate perpendicular to the wall is more delicate. Numerical experiments show that a Dirac delta function is unsuitable here owing to the oscillatory behaviour of the adjoint eigenfunction of the Orr–Sommerfeld equation. This behaviour will make the results strongly dependent on the distance from the source to the wall; see (12). Therefore a smooth distribution must be employed. Unfortunately, to date, experimental results are only available for the component of the Reynolds-stress tensor corresponding to the fluctuating transport of streamwise momentum in the direction perpendicular to the wall (Kim *et al.* 1971; Brodkey *et al.* 1974). Although this is the only component affecting the momentum balance for the mean velocity field, the remaining five components may very well have a strong influence on the fluctuating field. This influence will not average out in quadratic quantities such as energy spectra. Be that as it may, in order to be able to proceed, one must at present assume that the uv component provides the most efficient excitation of the fluctuations. The remaining components are accordingly set equal to zero. It is hoped that this highly simplified model will contain some of the essential physics of the problem posed.

The formerly mentioned measurements of uv during bursting show that this quantity is a weakly, but still noticeably, varying function of the outer Reynolds number. The measurements by Brodkey *et al.* (1974) were performed by using hot-wire anemometry and conditional sampling techniques. The raw data were processed on a computer. These results can be expected to be somewhat more accurate than those of Kim *et al.* (1971), who used visual techniques. However, the latter experiments were performed at a higher outer Reynolds number, and were thus considered to be more suitable for the present purpose.

The dependence of uv on y is here assumed to be the form

$$uv \sim c_1 y^3 \exp(-c_2 y^2), \tag{14}$$

where the adjustable constants c_1 and c_2 are computed from a least-squares fit to measured data.† The function uv with $c_1 = 1{\cdot}87 \times 10^{-3}$ and $c_2 = 4{\cdot}42 \times 10^{-3}$ is shown in figure 2, where the data from Kim *et al.* (1971) are also displayed. The third power of the distance from the wall appearing in (14) is a consequence of

† As the results to be presented in § 6 are normalized spectra, the value of c_1 is immaterial.

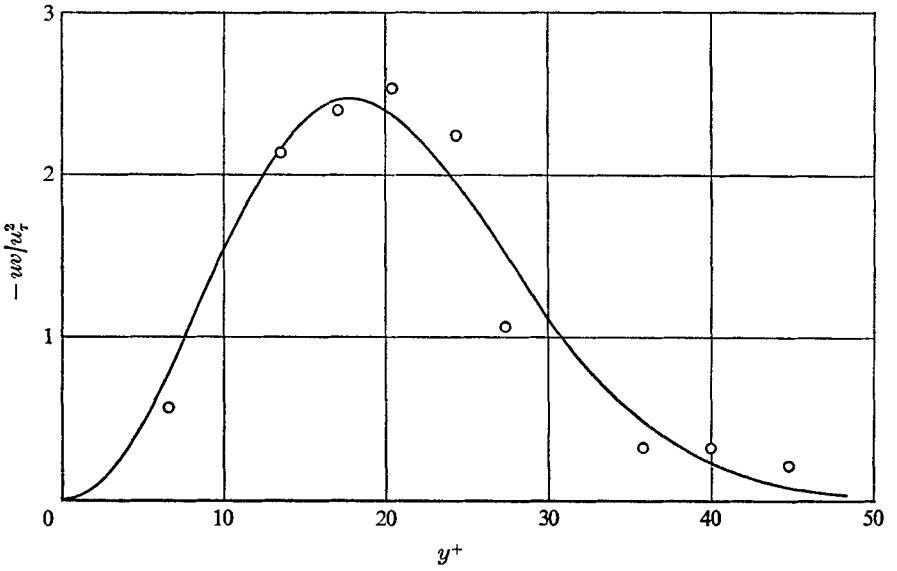

FIGURE 2. The uv component of the Reynolds-stress tensor as function of y^+ during bursting. O, measured points from Kim *et al.* (1971); ——, fitted curve according to formula (14).

continuity and the fact that u varies linearly with y near the wall (Hinze 1957, p. 472). The second power of y in the exponent in (14) was chosen because it gave a somewhat better fit to the data than did an expression containing the first power. If the motions producing Reynolds stress were weak, the behaviour of uv at large distances from the wall would be a very nearly exponential decay. However, the detailed dependence on y in this region should not matter very much because the adjoint eigenfunction in the integrand in (12) is here very small. The model for the behaviour in space-time of the instantaneous Reynolds stress is thus assumed to be of the form

$$uv = \delta(t)\,\delta(x)\,\delta(z)\,c_1 y^3 \exp(-c_2 y^2) \tag{15}$$

for each individual burst. The remaining components are assumed to have negligible influence.

In order to complete the modelling of the forcing term $\hat{Q}$ in (12) for the purpose of computing spectra, its statistics have to be considered. It is assumed here that the statistical properties of the turbulent flow field may be modelled analogously to the 'shot noise' current flowing in a resistor connected to a vacuum diode owing to the randomly occurring electron emission from the heated cathode. It is also assumed that the bursts occur independently in time and the homogeneous space co-ordinates. This approach has been used by, among others, Lumley (1965), Lahey & Kline (1971) and Kovasznay (1973). Such a stochastic process can in the one-dimensional case be written as

$$i(t) = \sum_m j_m H(t-t_m) = \sum_m F_m(t-t_m), \tag{16}$$

where H is the Heaviside unit step function. j_m and t_m are random variables whose probability distributions are assumed to be known. For the shot-noise problem

the coefficients j_m are equated to unity and it can be shown that t_m is given by a Poisson distribution. More general processes can be modelled by multiplying each term in the series (16) by some function of $t-t_m$. If a Poisson distribution is assumed also for j_m and $\langle i \rangle$ is assumed to be zero, the following relation can be shown to hold (Rice 1944):

$$\langle i(t)\, i(t+T)\rangle / \langle i^2 \rangle = \langle F(t)\, F(t+T)\rangle / \langle F^2 \rangle, \tag{17}$$

where the brackets stand for time averaging. This means that the statistics for the response function $i(t)$ are given by the response $F(t)$ of an individual event. For the present turbulence model this implies that the normalized energy spectrum of the fluctuating streamwise velocity component is given by the normalized spectrum of the response to an individual burst. It is implicitly assumed here that the temporal and spatial structure is the same for all bursts, whose strengths are assumed to be Poisson distributed. However, the visual observations of bursting motions by Kline *et al.* (1967) and Corino & Brodkey (1969) showed that this is certainly not true. These experiments clearly showed that there is a considerable variation in both the kinematics and strength of the motions which make the largest contribution to the Reynolds stress. Thus the results obtained must be interpreted with extreme care when this model for the fluctuating small-scale field is used. Only overall properties of the computed spectra can be expected to be reasonably well modelled. One consequence of the simplifying assumptions made is that, as will be seen below, the peaks in the computed spectra will be sharper than the measured ones. This is because the computed peaks are associated with the vertical scale of the particular model burst chosen. Improved results would most likely be obtained if the constants c_1 and c_2 in (14) were taken as random variables, but this would considerably complicate the numerical computations.

Moreover, experiments by Rao *et al.* (1971) indicated that the time between bursts is distributed according to a lognormal law. The probability density for the time between events at a fixed point in space for such a process is given by

$$f_1(t) = \frac{1}{(2\pi)^{\frac{1}{2}}\sigma t} \exp\left(\frac{-(\ln t - m)^2}{\sigma^2}\right), \tag{18}$$

where m is the mean value and σ the variance for the logarithm of the random variable t. For a Poisson process the probability density reads

$$f_2(t) = \lambda^{-1} \exp(-t/\lambda), \tag{19}$$

where λ is the mean value. Comparing (18) and (19) one sees that the most probable time between bursts for the Poisson-process model is zero whereas for the lognormal process this quantity is non-zero. This means that the bursts occurring at a given point fixed in space are not independent of each other (cf. Offen & Kline 1974). If a Poisson distribution is used the error is likely to be particularly serious for small scales. The behaviour for large values of t of the two probability density functions is also different, but this is presumably not so serious as the difference for small t. It can thus be expected that anomalous behaviour of the computed wavenumber spectra may show up for high frequencies. The reason

for this is that a Poisson-process model will overestimate the amount of small scales present in the field because according to this model bursting would occur too often. If the more realistic lognormal model is used, the surplus of small scales will have time to decay between bursting events. The assumption that the joint space–time statistics are such that the probability distribution can be written as a product of three functions each depending on one variable only is also unrealistic. The experiment by Kline *et al.* (1967) indicated very clearly that the bursting motions are closely connected with the streamwise streaks, which in turn were shown to occur in a rather well-defined periodic pattern in the spanwise direction. However, because of the considerable simplifications to the mathematics offered by (17) if this assumption is made, as suggested by Kovasznay (1973), such a Poisson distribution both in time and the homogeneous co-ordinates is assumed also in this work to model the statistics of the bursting motions.

The assumption of a Dirac delta function behaviour in time and the homogeneous co-ordinates for each individual burst will also cause non-physical behaviour of the computed spectra at large distances from the origin in frequency–wavenumber space, i.e. for scales of the order of the burst motion itself.

6. Computation of spectra

Combining (8) and (9) with the continuity equation and employing the form for $\hat{v}$ found from (12) one can solve for $\hat{u}$ and then determine the frequency–wavenumber spectrum in the standard manner. The result reads

$$S_{uu}(y, \omega, k_x, k_z) = \sum_{n,\,m} \hat{u}^{(n)} \hat{u}^{(m)*}, \tag{20}$$

where $*$ denotes the complex conjugate,

$$\hat{u}^{(n)} = \frac{ik_x}{k^2} D\hat{v}^{(n)} + \frac{k_z k_x}{k^2} \tilde{w}^{(n)}, \tag{20a}$$

$$\tilde{w}^{(n)} = L^{-1}[(ik_z/k_x)(DU)\hat{v}^{(n)}] + \tilde{w}_H \tag{20b}$$

and the operator L and $\tilde{w}_H$ are defined by

$$L[\tilde{w}_H] = [(U-c) + (i/k_x R)(D^2 - k^2)]\tilde{w}_H = 0. \tag{21}$$

The homogeneous solution $\tilde{w}_H$ has to be included in order to satisfy the condition of zero slip at the wall. In deriving (20*b*), the last term in (11) was neglected as explained in § 4, since it does not contribute wavelike terms. The series (20) is in this calculation terminated after the first term under the assumption that the higher eigenmodes do not contribute significantly to the statistics owing to their high decay rates (cf. Landahl 1967). According to § 5 the formula (20) also gives the spectrum for the disturbance field as a whole for the statistical model chosen. Although the spectrum for the normal fluctuating velocity would be considerably easier to compute, the u spectrum was chosen for several reasons. The u component plays, according to the present turbulence model, a key role in the maintenance of the turbulent flow field because it intermittently creates conditions for the occurrence of momentum-transporting bursting motions.

Knowledge of the length and time scales of this component should thus provide some information on the average intervals in time and space between bursts. Furthermore, the normal component is difficult to measure very near a solid surface and there seem to be no frequency–wavenumber spectra of this component measured in the wall region available in the literature, whereas a substantial amount of such data has been presented for the u component (Morrison & Kronauer 1969; Morrison *et al.* 1971). For these reasons, only spectra of the fluctuating streamwise velocity component are considered in the following. The two- and one-dimensional normalized spectra are defined as

$$\bar{\bar{S}}_{uu}(\omega, k_x) = V^{-1}\int S_{uu}(\omega, k_x, k_z)\,dk_z, \tag{22a}$$

$$\bar{\bar{S}}_{uu}(\omega, k_z) = V^{-1}\int S_{uu}(\omega, k_x, k_z)\,dk_x, \tag{22b}$$

$$\bar{S}_{uu}(\omega) = V^{-1}\iint S_{uu}(\omega, k_x, k_z)\,dk_x\,dk_z, \tag{22c}$$

$$\bar{S}_{uu}(k_x) = V^{-1}\iint S_{uu}(\omega, k_x, k_z)\,d\omega\,dk_z, \tag{22d}$$

$$\bar{S}_{uu}(k_z) = V^{-1}\iint S_{uu}(\omega, k_x, k_z)\,d\omega\,dk_x, \tag{22e}$$

$$V = \iiint S_{uu}(\omega, k_x, k_z)\,d\omega\,dk_x dk_z, \tag{22f}$$

where the dependence on y is dropped for brevity. In the following the overbars in the definitions of the two- and one-dimensional spectra are dropped since no confusion can arise thereby. The numerical results are presented in the usual wall units.

The spectra defined by (22*a–f*) have been computed at a height of 15 wall length units above the plate on the following mesh in frequency–wavenumber space:

$$0{\cdot}01 \leqslant \omega^+ \leqslant 0{\cdot}61, \quad \Delta\omega^+ = 0{\cdot}03,$$

$$0{\cdot}005 \leqslant k_x^+ \leqslant 0{\cdot}03, \quad \Delta k_x^+ = 0{\cdot}005,$$

$$0{\cdot}005 \leqslant k_z^+ \leqslant 0{\cdot}105, \quad \Delta k_z^+ = 0{\cdot}005.$$

Upstream 'propagation' of Fourier components, signified by the frequency and wavenumber having opposite signs, is thus not considered. The two- and one-dimensional spectra were computed from the three-dimensional spectrum by a multi-dimensional Simpson formula. The reason for the particular choice of the height above the wall ($y^+ = 15$) made is that experiments have shown that this is near the region where the turbulent production and the root mean square of the streamwise velocity fluctuation attain their maximum values (Kline *et al.* 1967). Furthermore, the convection velocity of the streamwise velocity fluctuations matches the mean velocity in the neighbourhood of this point (Morrison *et al.* 1971).

The computations were in fact carried out to higher streamwise wavenumbers than those given above. However, it was found that for larger values of k_x^+ the spectrum started to grow with increasing k_x^+ and to oscillate with k_z^+ for wavenumbers corresponding to a typical burst size. These results were judged to be physically insignificant and were therefore discarded. There are several reasons for such anomalous behaviour of the computed spectra.

(i) As was pointed out in the foregoing section, the model (15) used for the Reynolds stress during a burst is strongly oversimplified in its dependence on the homogeneous co-ordinates and time. If the forcing term had been more realistically described, say by a product of Gaussian bell-shaped functions in these co-ordinates having small but finite widths, the influence of high frequencies and wavenumbers would have been reduced. This would have required additional parameters in the model and was therefore discarded in favour of delta functions.

(ii) From the expression for $\hat{Q}$ one sees that the second derivative with respect to y^+ of the difference between the instantaneous Reynolds stress and its mean value is required to compute the response according to (12). After integration by parts one then finds that the fit to the measured dependence of $\hat{Q}$ on y^+ will be multiplied by the second derivative of the adjoint eigenfunction. Because of the oscillatory behaviour of this function for high wavenumbers, large errors are likely to occur in this region.

(iii) The statistical model will overemphasize the influence of small scales. This is probably the most serious limitation of the model and was discussed in § 5.

From the above remarks it is obvious that the computed results in the high wavenumber regime are very sensitive to errors in the fine-structure of the burst model. Further improvements are sorely needed on this point. In order to investigate this matter, some numerical experiments were carried out where the response to some other types of momentum sources were computed. It was found that common to all the results from these numerical experiments was the occurrence of a sharp peak in the low wavenumber region. The wavenumbers for this maximum were found to differ only by amounts of order unity for different source functions. The behaviour of the computed spectra for large streamwise wavenumbers, did, however, differ considerably.

7. Properties of the computed spectra

The computed one- and two-dimensional spectra are shown in figures 3 and 4. In general, great caution should be exercised when trying to interpret long-time averaged energy spectra of a random field. Such spectra contain nothing more than information on the average distribution of scales. An illuminating analysis of the loss of information due to long-time averaging has been given by Lahey & Kline (1971).

The k_x^+ spectrum shown in figure 3 (*a*) indicates that the large-scale response to the particular burst model chosen can be interpreted as a rather well defined wave packet. The peak of the computed spectrum is reasonably close to the one measured by Morrison *et al.* (1971). This is also true for the k_z^+ spectrum shown in figure 3 (*b*). An interesting result which can be inferred from this graph is that by far the greatest part of the energy of the excited field is projected on highly swept waves. This is also in agreement with the experimental results of Morrison *et al.* (1971), who showed that the observed streaky structure near the wall could be explained by the presence of a system of waves steeply inclined to the mean flow. Also the computed frequency spectrum shown in figure 3 (*c*) displays approximately the correct time scale for the large eddies in the wall layer.

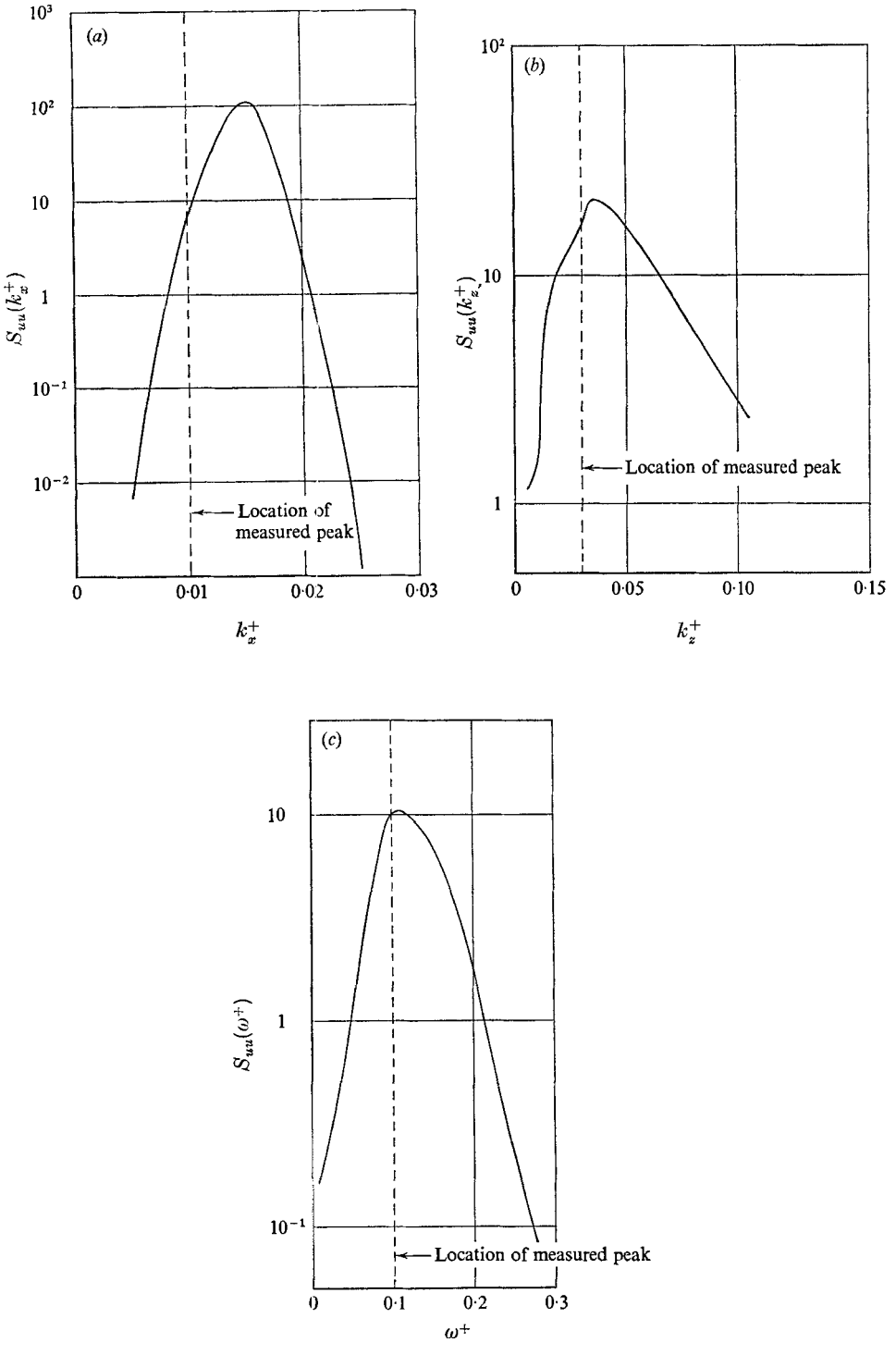

FIGURE 3. (*a*) $S_{uu}(k_x^+)$, (*b*) $S_{uu}(k_z^+)$ and (*c*) $S_{uu}(\omega^+)$ computed at $y^+ = 15$. Location of the measured peak from Morrison *et al.* (1971).

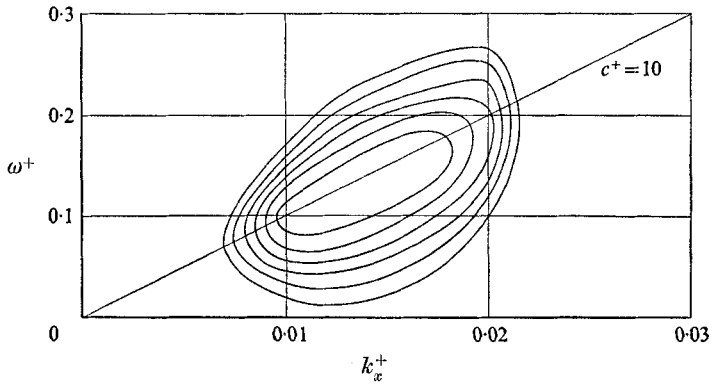

FIGURE 4. $S_{uu}(\omega^+, k_x^+)$ computed at $y^+ = 15$. The values on two consecutive level curves differ by a factor of 2.

The three-dimensional u spectrum has a pole at the complex frequency given by the eigenvalues for each given pair of spanwise and streamwise wavenumbers. Additional singularities emanate from the operator L_w^{-1} in (20). Whether the latter are important or not may be investigated by separating out the influence of the pole at $\omega^+ = \omega^{(0)+}$ by setting

$$S_{uu}(\omega^+, k_x^+, k_z^+) = Z(\omega^+, k_x^+, k_z^+)/|\omega^+ - \omega^{(0)+}|^2, \tag{23}$$

where Z will contain the influence of the other singularities. For the one-dimensional frequency spectrum we accordingly define a quantity $\hat{Z}$ by

$$\hat{Z} = \int |\omega^+ - \omega^{(0)+}|^2 S_{uu}(\omega^+, k_x^+, k_z^+)\, dk_x^+ dk_z^+, \tag{24}$$

the variation of which with ω^+ will indicate the importance of the remaining singularities. In figure 5 $\hat{Z}(\omega^+)$ and $S_{uu}(\omega^+)$ are plotted; $\hat{Z}$ is normalized to the same value as $S_{uu}(\omega^+)$ at the left end-point of the interval. From this graph it can be seen that $\hat{Z}$ is a slowly varying function of ω^+, showing that the importance of the remaining singularities is small in the interval considered. As the variation of $\omega^{(0)+}$ with k_z^+ near the peak in $S_{uu}(k_z^+)$ is also small, see figures 3 (*b*) and 7, an approximate formula for $S_{uu}(\omega^+, k_x^+)$ would be

$$S_{uu}(\omega^+, k_x^+) \simeq \tilde{Z}(k_x^+)/|\omega^+ - \omega^{(0)+}|^2, \tag{25}$$

where

$$\tilde{Z} = \int \hat{Z}\, dk_x^+. \tag{26}$$

According to (25) the energy distribution in the k_x^+, ω^+ plane should be located in a band around the curve defining the phase velocity. The width of this band will essentially be determined by the diffusive properties of the waves, i.e. the imaginary part of the eigenfrequency. The computed k_x^+, ω^+ spectrum is shown in figure 4 and the same spectrum measured by Morrison *et al.* (1971) is shown in figure 6. In figure 4 the line corresponding to the experimentally found convection velocity is also shown. From these graphs it can be seen that the characters of the computed and measured spectra are rather similar. The main difference is in the energy distribution as function of k_x^+, which has a much sharper

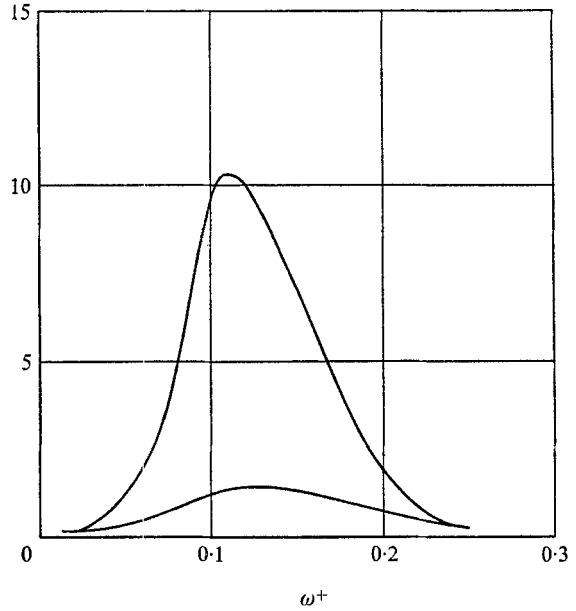

FIGURE 5. $S_{uu}(\omega^+)$ (upper curve) and $\hat{Z}(\omega^+)$ (lower curve), defined by (24).

peak in the computed spectra than in the measured one. As was discussed in § 3, this is very likely a consequence of the assumption that all bursts have the same vertical structure.

The computed real and imaginary parts of the streamwise phase speed as functions of the streamwise wavenumber for different spanwise wavenumbers are shown in figure 7. This diagram indicates that all waves are damped. Büssman & Münz (1942) have estimated the stability boundary for the model velocity profile used, given by (3), to be $a \simeq 2{\cdot}6 \times 10^2$, which means that all waves are indeed highly stable. The imaginary part of the phase speed seems to be roughly independent of the wavenumber, and the result of Landahl (1967) that each eddy has a lifetime proportional to its size is thus found to be valid for long waves in the wall layer as well. The e-folding time of each wave is approximately one third of its period. This means that during decay the peak in the energy spectrum for each eddy will successively move towards lower frequencies and wavenumbers. Also the real part of the streamwise phase velocity is roughly constant, which means that the group velocity is approximately equal to the phase velocity and that dispersion is weak for this waveguide. The small dispersivity means that the temporal variation of a wave packet as it travels downstream is almost exclusively caused by the different e-folding times of each component. The decay mechanism is provided by the interaction of each wave with the mean flow and, as $k_x R$ is here of order one, viscous diffusion. The computed dispersion relation also shows that the frequency depends only weakly on the spanwise wavenumber, so that the lateral spread of influence is small for the first mode in (20). As suggested by Morrison *et al.* (1971), one may interpret spectra of the kind shown in figures 3 and 4 as emanating from vortices nearly aligned with the mean flow. It should be

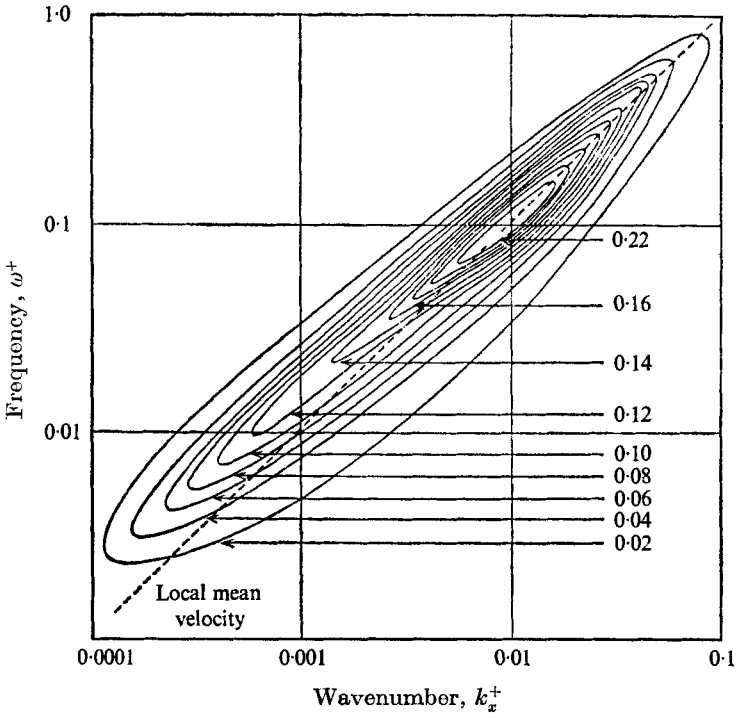

FIGURE 6. Measured $S_{uu}(\omega^+, k_x^+)$. From Morrison *et al.* (1971).

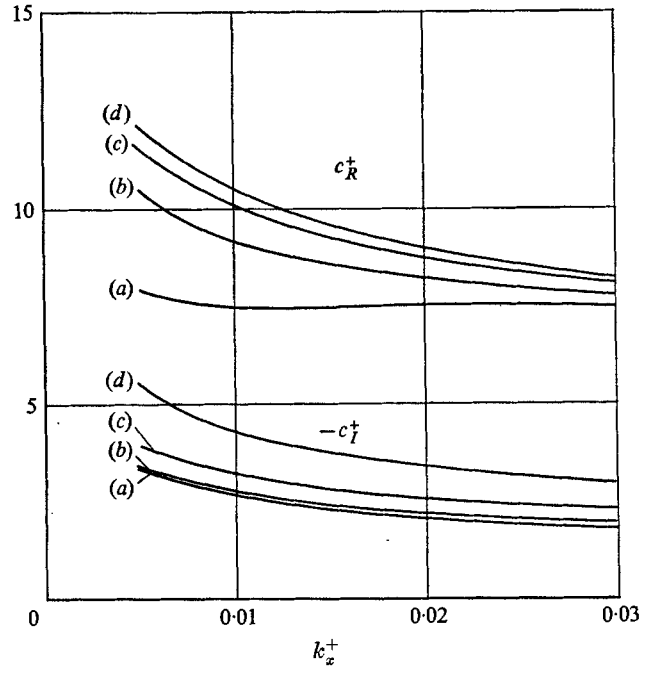

FIGURE 7. Computed phase velocity as function of k_z^+. (*a*) $k_z^+ = 0{\cdot}005$. (*b*) $k_z^+ = 0{\cdot}025$. (*c*) $k_z^+ = 0{\cdot}05$. (*d*) $k_z^+ = 0{\cdot}1$.

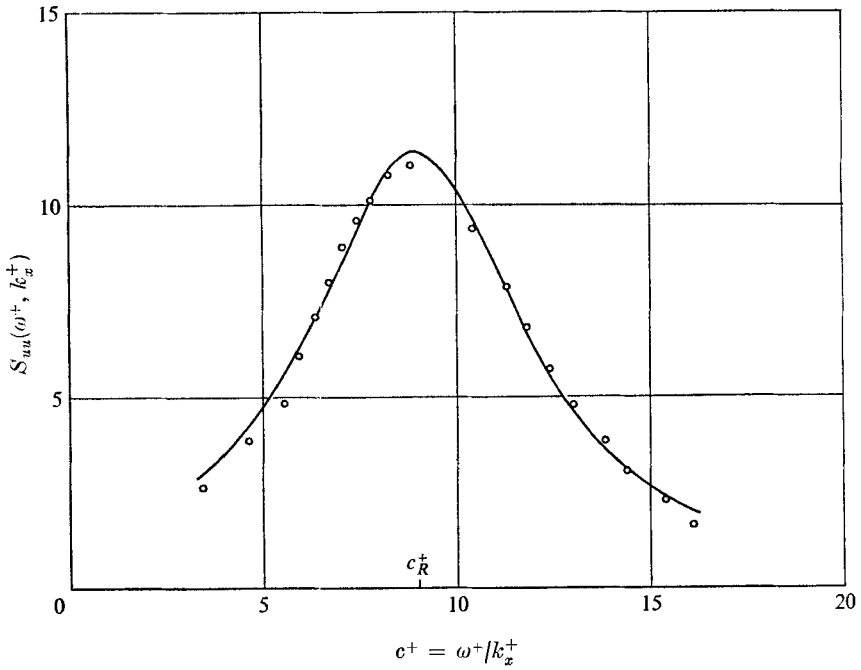

FIGURE 8. O, measured values of $S_{uu}(\omega^+, k_x^+)$ for $k_x^+ = 0{\cdot}01$ from Morrison *et al.* (1971); ——, three-parameter fit according to (25).

pointed out that this type of flow pattern in turbulent shear flows was first suggested by Townsend (1956, p. 208).

The consistency of the present calculations can be investigated by fitting a three-parameter expression of the form (25) to sections parallel to the frequency axis through the k_x^+, ω^+ spectra measured by Morrison *et al.* (1971). Such a fit is shown in figure 8. From these fits one obtains, assuming the model to be valid, experimentally determined values for $c^{(0)+} = c_R^{(0)+} + ic_I^{(0)+}$ for different k_x^+. These values can be compared with the computed wave-propagation constants for the spanwise wavenumber which gives the largest contribution to the integral in formula (26) for $\tilde{Z}$. Such a comparison is shown in figure 9, from which it can be seen that the model indeed seems to be consistent with the experimental data. Thus, as in a simple second-order mechnical system, the frequency bandwidth may be interpreted as a decay rate.

The absolute values of the three perturbation velocity components as functions of y^+ for the most energetic wavenumber vector and frequency at $y^+ = 15$ are shown in figure 10. This graph may be compared with figure 11, which is a re-plot by Schubert & Corcos (1967) of the same quantities from the measurements by Klebanoff (1954). From these graphs it can be seen that the model gives the correct relative magnitudes of the different components in the region where it can be expected to hold approximately. The much sharper peak in the computed streamwise velocity fluctuation as compared with the measured values can be explained in the same way as for the spectra; see above.

The structure of the fluctuating streamwise velocity field found here is similar

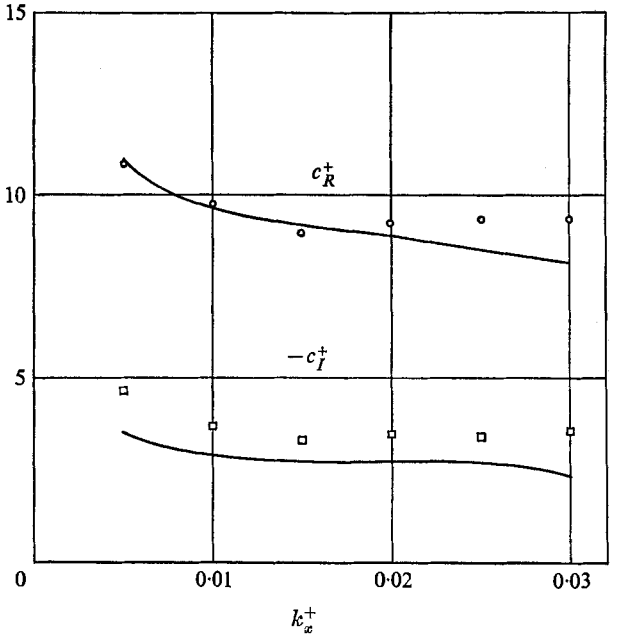

FIGURE 9. Real and imaginary parts of the downstream phase velocity. ○, □, computed from (25) and measurements by Morrison *et al.* (1971); ——, computed from the Orr–Sommerfeld equation.

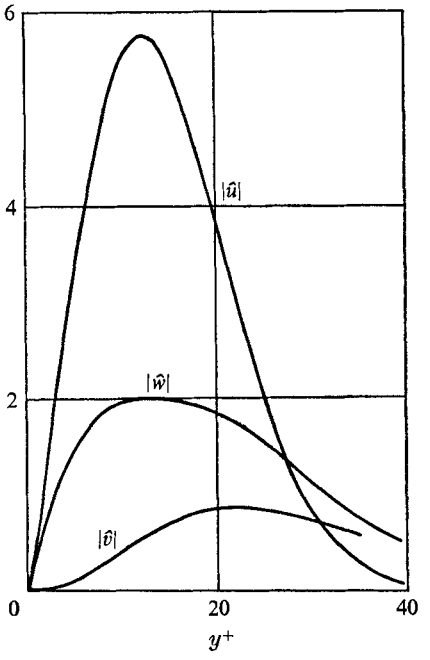

FIGURE 10. Computed absolute values of the fluctuating velocity components for the wavenumber at the peaks of the spectra in figures 3(*a*) and (*b*).

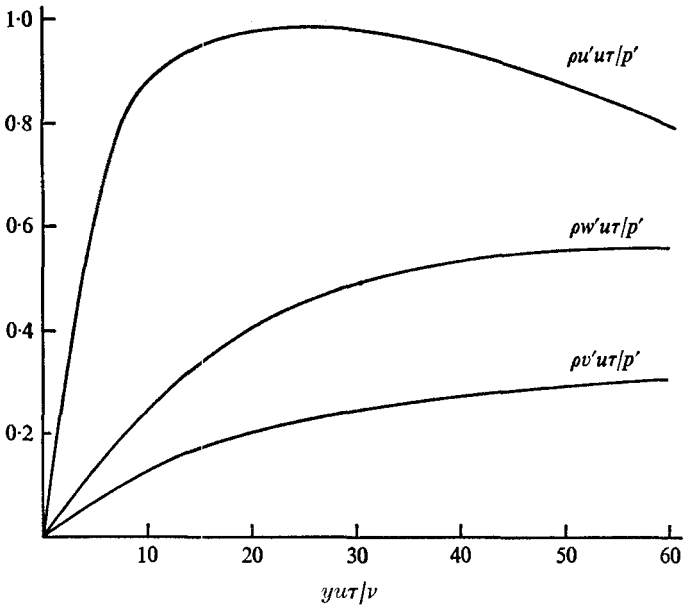

FIGURE 11. Measured r.m.s. values of the fluctuating velocity component by Klebanoff (1954). From Schubert & Corcos (1967).

to that obtained by Bakewell & Lumley (1967). These authors measured two-point correlations near the wall in a turbulent pipe flow of glycerine. They decomposed their data according to the proper orthogonal decomposition theorem (Lumley 1965) and computed, after making use of an eddy-viscosity hypothesis, a pattern consisting of two counter-rotating vortices as the dominant eddies near the wall. This pair of vortices would occur randomly in time and space. The spanwise separation between the centres of the computed vortices agreed very well with measurements by Kline *et al.* (1967). Bakewell & Lumley were not able to predict from their work the streamwise scale or characteristic time of the eddies. However, their model could in principle be used to find such scales if the correlations in all three space co-ordinates and time were available. Another difference between results of the work by Bakewell & Lumley (1967) and the present investigation is that the former authors regarded the vorticity of the eddies as being convected by the mean flow whereas according to the present model this vorticity propagates.

8. Conclusions

By using highly simplified models for the mean velocity distribution and the intermittent Reynolds stress in the wall region of a turbulent boundary layer, energy spectra of the fluctuating large-scale motions in this region have been computed. The computed length and time scales were found to be in good agreement with experimental data. The agreement is perhaps somewhat fortuitous considering the rather crude model used, but one can anyway conclude that the physical mechanism suggested for the production of large eddies in the wall

layer is reasonable. However, the computed wavenumber spectra display narrower bandwidths than the measured ones. This is a consequence of the crudeness of the model for the intermittent Reynolds stress. According to the present model calculations the statistically dominant velocity fluctuations in the wall layer consist of wave packets having a significant amount of streamwise vorticity. These wave packets are produced randomly in space and time by the intermittent Reynolds stress and propagate downstream. The results are qualitatively similar to those of Bakewell & Lumley (1967).

This paper reports a portion of the author's doctoral thesis (Bark 1974). The author is very grateful for many clarifying and inspiring discussions of the subject with Professor Marten Landahl. Prof. Louis N. Howard also provided many valuable points of view. Prof. Richard Kronauer very kindly made available an enlarged copy of figure 7. This work was sponsored by the Swedish Board of Technical Development and by Eriksberg's Shipyard.

REFERENCES

BAKEWELL, H. P. & LUMLEY, J. L. 1967 *Phys. Fluids*, **10**, 1880.

BARK, F. H. 1974 Ph.D. thesis, Dept. Mech., Roy. Inst. Tech., Stockholm.

BLACKWELDER, R. F. & KAPLAN, R. E. 1972 *AGARD Conf. Proc.* p. 93.

BRODKEY, R. S., WALLACE, J. M. & ECKELMANN, H. 1974 *J. Fluid Mech.* **63**, 209.

BÜSSMAN, K. & MÜNZ, H. 1942 *Jb. Dtsch. Luftfahrtf.* **1**, 36.

COLES, D. 1956 *J. Fluid Mech.* **1**, 191.

CORINO, E. R. & BRODKEY, R. S. 1969 *J. Fluid Mech.* **37**, 1.

ECKHAUS, W. 1965 *Studies in Non-Linear Stability Theory*. Springer.

GUPTA, A. K., LAUFER, J. & KAPLAN, R. E. 1971 *J. Fluid Mech.* **50**, 493.

HINZE, J. O. 1957 *Turbulence*. McGraw-Hill.

KIM, H. T., KLINE, S. J. & REYNOLDS, W. C. 1971 *J. Fluid Mech.* **50**, 133.

KLEBANOFF, P. S. 1954 *N.A.C.A. Tech. Note*, no. 3178.

KLEBANOFF, P. S., TIDSTROM, K. D. & SARGENT, L. M. 1962 *J. Fluid Mech.* **12**, 1.

KLINE, S. J., REYNOLDS, W. C., SCHRAUB, F. A. & RUNSTADLER, P. W. 1967 *J. Fluid Mech.* **30**, 741.

KOVASZNAY, L. S. G. 1973 *Symposia Matematica del Istituto Nazionale di Alta Matematica*, vol. 9, p. 507. Academic.

LAHEY, R. T. & KLINE, S. J. 1971 *Thermosci. Div., Dept. Mech. Engng, Stanford University, Rep.* MD-26.

LANDAHL, M. T. 1967 *J. Fluid Mech.* **29**, 441.

LANDAHL, M. T. 1972 *J. Fluid Mech.* **56**, 775.

LANDAHL, M. T. 1975 *SIAM J. Appl. Math.* (to appear).

LAUFER, J. & BADRI NARAYANAN, M. A. 1971 *Phys. Fluids*, **14**, 182.

LIGHTHILL, M. J. 1952 *Proc. Roy. Soc.* A **211**, 564.

LUMLEY, J. L. 1965 *Proc. Int. Coloq. on Fine-Scale Processes in the Atmosphere and Their Influence on Radio-Wave Propagation*. Moscow: Dokl. Akad. Nauk.

MORRISON, W. R. B., BULLOCK, K. J. & KRONAUER, R. E. 1971 *J. Fluid Mech.* **47**, 639.

MORRISON, W. R. B. & KRONAUER, R. E. 1969 *J. Fluid Mech.* **39**, 117.

OFFEN, G. R. & KLINE, S. J. 1974 *J. Fluid Mech.* **62**, 223.

RAO, K. N., NARASIMHA, R. & BADRI NARAYANAN, M. A. 1971 *J. Fluid Mech.* **48**, 339.

RICE, S. O. 1944 *Bell System Tech. J.* no. 23–24.

SCHUBERT, G. & CORCOS, G. M. 1967 *J. Fluid Mech.* **29**, 113.

SQUIRE, H. B. 1933 *Proc. Roy. Soc.* A **142**, 621.

STERNBERG, J. 1965 *AGARDograph*, no. 97, part 1, p. 1.

TOWNSEND, A. A. 1956 *The Structure of Turbulent Shear Flow.* Cambridge University Press.

WALLACE, J. M., ECKELMANN, H. & BRODKEY, R. S. 1972 *J. Fluid Mech.* **54**, 39.

WILLMARTH, W. W. & LU, S. S. 1972 *J. Fluid Mech.* **55**, 65.

WILLMARTH, W. W. & LU, S. S. 1973 *J. Fluid Mech.* **60**, 481.

WILLMARTH, W. W. & WOOLDRIDGE, C. E. 1962 *J. Fluid Mech.* **14**, 187.